Lab on a Chip

PAPER

View Article Online
View Journal | View Issue

Cite this: *Lab Chip*, 2023, **23**, 2434

Surface modifications of COP-based microfluidic devices for improved immobilisation of hydrogel proteins: long-term 3D culture with contractile cell types and ischaemia model†

Sandra González-Lana, [ac] Teodora Randelovic,[abd] Jesús Ciriza, [ab] María López-Valdeolivas,[e] Rosa Monge,[c] Carlos Sánchez-Somolinos [de] and Ignacio Ochoa *[abd]

The tissue microenvironment plays a crucial role in tissue homeostasis and disease progression. However, the *in vitro* simulation has been limited by the lack of adequate biomimetic models in the last decades. Thanks to the advent of microfluidic technology for cell culture applications, these complex microenvironments can be recreated by combining hydrogels, cells and microfluidic devices. Nevertheless, this advance has several limitations. When cultured in three-dimensional (3D) hydrogels inside microfluidic devices, contractile cells may exert forces that eventually collapse the 3D structure. Disrupting the compartmentalisation creates an obstacle to long-term or highly cell-concentrated assays, which are extremely relevant for multiple applications such as fibrosis or ischaemia. Therefore, we tested surface treatments on cyclic-olefin polymer-based microfluidic devices (COP-MD) to promote the immobilisation of collagen as a 3D matrix protein. Thus, we compared three surface treatments in COP devices for culturing human cardiac fibroblasts (HCF) embedded in collagen hydrogels. We determined the immobilisation efficiency of collagen hydrogel by quantifying the hydrogel transversal area within the devices at the studied time points. Altogether, our results indicated that surface modification with polyacrylic acid photografting (PAA-PG) of COP-MD is the most effective treatment to avoid the quick collapse of collagen hydrogels. As a proof-of-concept experiment, and taking advantage of the low-gas permeability properties of COP-MD, we studied the application of PAA-PG pre-treatment to generate a self-induced ischaemia model. Different necrotic core sizes were developed depending on initial HCF density seeding with no noticeable gel collapse. We conclude that PAA-PG allows long-term culture, gradient generation and necrotic core formation of contractile cell types such as myofibroblasts. This novel approach will pave the way for new relevant *in vitro* co-culture models where fibroblasts play a key role such as wound healing, tumour microenvironment and ischaemia within microfluidic devices.

Received 26th January 2023,
Accepted 17th March 2023

DOI: 10.1039/d3lc00075c

rsc.li/loc

Introduction

Cell culture has been one of the most used preclinical models for decades. It has evolved from conventional and traditional bi-dimensional to the most advanced three-dimensional (3D) based models. The new models try to resemble, as much as possible, the pathophysiological *in vivo* cellular behaviour. *In vivo*, cells embedded or surrounded by a 3D architecture are influenced by different biochemical and mechanical stimuli, depending on the cell type and tissue. Thus, the 3D microenvironment enhances interactions among neighbouring cells and extracellular matrix (ECM), influencing pathophysiological cell motility, proliferation, migration, and morphology.[1–3] In the last decades, several 3D culture systems have been developed[4–6] trying to mimic the

[a] *Tissue Microenvironment (TME) Lab. Aragón Institute of Engineering Research (I3A), University of Zaragoza, C/ Mariano Esquillor s/n, 500018 Zaragoza, Spain. E-mail: iochgar@unizar.es*
[b] *Institute for Health Research Aragón (IIS Aragón), Paseo de Isabel La Católica 1-3, 50009 Zaragoza, Spain*
[c] *BEONCHIP S.L., CEMINEM, Campus Río Ebro. C/ Mariano Esquillor Gómez s/n, 50018 Zaragoza, Spain*
[d] *CIBER in Bioengineering, Biomaterials and Nanomedicine (CIBER-BBN), Madrid, Spain*
[e] *Aragón Institute of Nanoscience and Materials (INMA), Department of Condensed Matter Physics (Faculty of Science), CSIC-University of Zaragoza, C/ Pedro Cerbuna 12, 50009 Zaragoza, Spain*

† Electronic supplementary information (ESI) available. See DOI: https://doi.org/10.1039/d3lc00075c

complex tissue microenvironment. However, although spheroids, organoids, scaffolds based on hydrogels and 3D bioprinted-based models provide closer *in vivo* scenarios than cell monolayers, they do not entirely resemble the microenvironmental characteristics.[7–10] They present limitations such as lack of vasculature and mechanical stimulation, imprecise control over gradients, or limited medium exchange at discrete points.[11] These disadvantages have been overcome by coupling the aforementioned 3D cultures with microfluidic devices (MD). The compartmentalisation of chambers and channels in a micrometric scale allows spatial control, resembling the *in vivo* microenvironmental cell distribution more closely.[12,13] Moreover, microfluidic devices allow perfusing medium adjacent to or through a cell culture with a stable nutrient and oxygen supply, waste removal and generating chemical gradients. They also allow exerting mechanical forces such as shear stress and interstitial pressure, affecting the cellular morphology and gene expression.[14–16] Optical monitoring in microfluidic devices also facilitates easy measurements due to the microfluidic channels defined heights that lead to a controlled focal distance between the sample and the optical objective. Matrices or scaffolds to support 3D cell cultures inside microfluidic device chambers should mimic the spatial complexity and mechanical properties of *in vivo* microenvironment. In natural protein matrices, cells can migrate through the fibrillar network by a motion of non-crosslinked collagen. Thus, cells bind to ECM through integrin and focal adhesion points, exerting active contractility and mechanosensing.[17,18] The interaction with integrins is transduced to biochemical signals that lead to cell attachment, migration or ECM remodelling. If the hydrogel has insufficient resistance to the cell-applied force, it deforms, modifying its initial geometry that might eventually lead to a collapse (Fig. 1).[19–21] This hydrogel collapse can be noticed as an *X*–*Y* hydrogel detachment (top view) from the microfluidic device walls (Fig. 1A), or just with a *Z* axis contraction (Fig. 1C, section view of Fig. 1B). Therefore, the analysis of the three axes is required to monitor the evolution of the gel integrity over time (Fig. 1D, non-contracted gel). Collagen-based hydrogel contraction and remodelling is a natural outcome of cellular expansion and interaction with the matrix.[22–24] However, this phenomenon may ruin the hydrogel architecture within the microfluidic device,[25] disrupting the compartmentalisation and affecting chemical gradients (ESI† Fig. S1).

The techniques to improve the bonding between the device and the ECM protein to prevent hydrogel contraction in microfluidic devices can be classified into three main groups: physical adsorption (physisorption), covalent bonding and their combination.[26] In physical adsorption, proteins are adsorbed to the surface by intermolecular forces (electrostatic, hydrophobic, van der Waals, hydrogen bonding interactions or combination). Surface oxidation is the most common method used to condition the surface. For covalent protein bonding, among others,[27] silanization and grafting, with alkoxy- or chloro-silanes, such as 3-aminopropyltriethoxysilane (APTES)[28–30] that later is covalently bonded to the protein. Another treatment used for covalent immobilisation consists of the ultraviolet (UV)-graft polymerisation with benzophenone as photoinitiator and, for example, acrylic acid (AA) to produce polyacrylic acid (PAA) brushes on the surface[26,31] to which the proteins are subsequently covalently linked. The combination of two or more immobilisation mechanisms is possible. Thus, physisorption and covalent bonding might be performed by adsorbing positively charged molecules such as poly-D-lysine (PDL) or poly-L-lysine (PLL) on activated surfaces, further activating them for covalent protein immobilisation.[32,33]

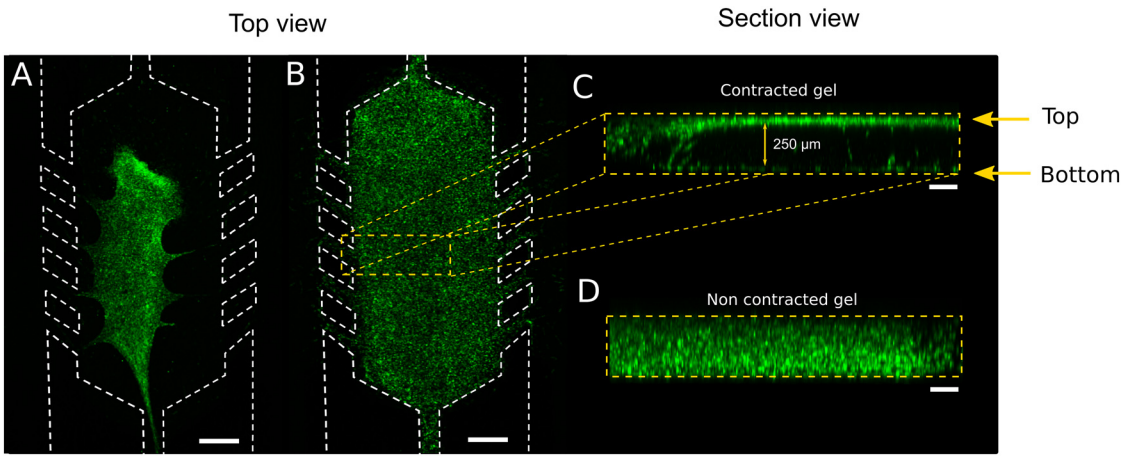

Fig. 1 3D culture of green labelled fibroblasts embedded in collagen hydrogel in a microfluidic device. Confocal top view micrograph of (A) collapsed collagen embedded cells and (B) apparently conserving the 3D structure. (C) Section view of the culture chamber by confocal *Z*-stacks reconstruction images of the hydrogel from B showing a non-homogeneous cell distribution, that tends to localise on the walls of the device. (D) Section view of the culture chamber of a non-contracted gel with cell homogeneously distributed along the height of the chamber. Note: scale bar 500 μm (A and B), 100 μm (C and D). Height of the section in (C) and (D) 250 μm.

The aforementioned methods for protein immobilisation have been mainly validated for PDMS-based microfluidic devices. PDMS is widely used in microfluidics because of its high biocompatibility, optical transparency, gas permeability, malleability and easy prototyping. Nonetheless, thermoplastic materials such as cyclic olefin polymer (COP) and cyclic olefin copolymer (COC) are becoming materials of great interest. These low-cost materials can be massively produced with mould-based techniques, such as injection moulding or hot embossing. Moreover, they are considered medical-grade plastics, with very low gas permeability, resistance to solvents, acids and bases, heat resistance, excellent optical properties, and no unspecific adsorption issues.[26] COP and COC are available from various vendors under different brand names (Topas®, Apel®, Zeonor® and Zeonex®) and grades. Depending on the monomers included, their ratios, molecular weight as well as the presence of additives, different material properties can be tuned to some extent adapting their performance to different applications.[34] Although the hydrophobicity of native cyclic olefin (co) polymers represents a great challenge for the use of these materials in microfluidic applications and as cell culture platforms, their surface can be modified to increase hydrophilicity and create functional groups for the attachment of biological entities.[35]

Protein immobilisation by silanization[36–38] and polyacrylic photografting have never been applied on COP-based microfluidic devices (COP-MD)[39–42] to preserve the three-

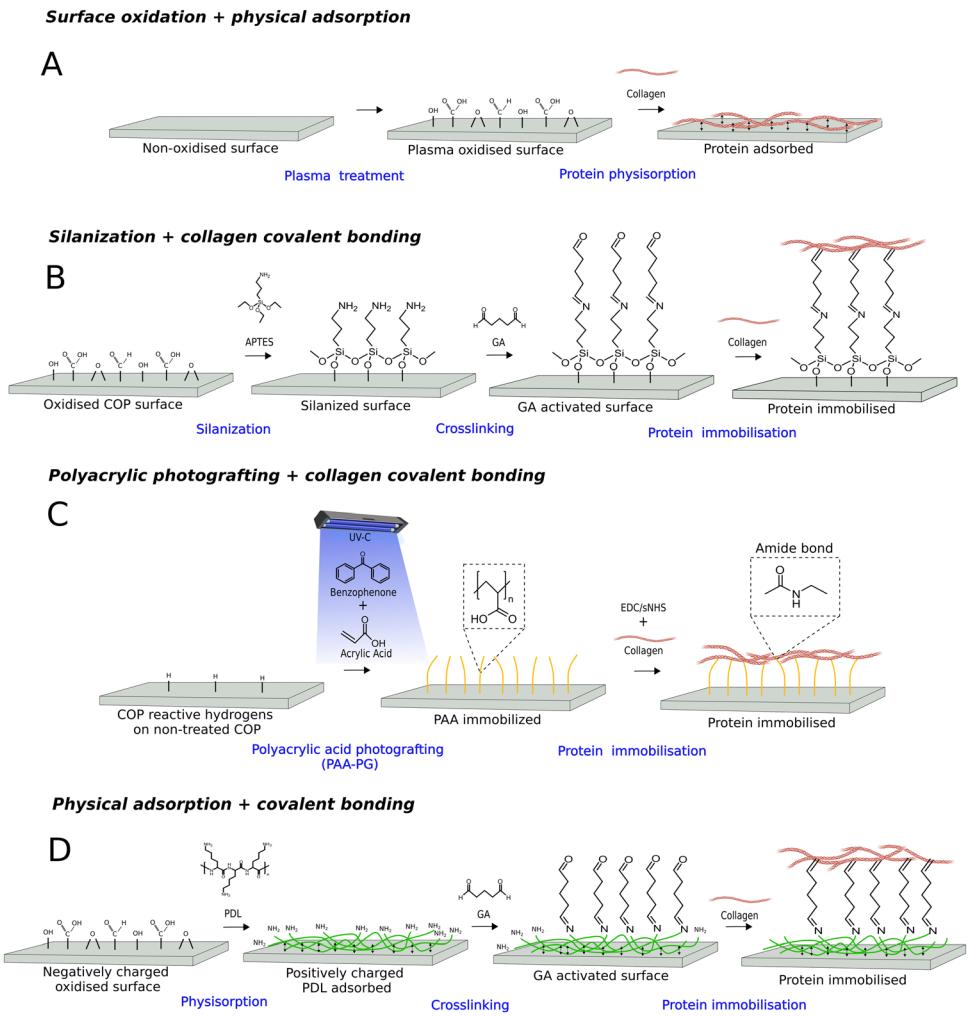

Fig. 2 Schematic illustration of COP surface modification procedures involved in collagen gel immobilisation. A) Oxygen plasma activates the inert surface of the COP by oxidizing and inducing the formation of polar functional groups carboxyl (C–O, C═O) and hydroxyl (–OH). It increases the hydrophilicity of the material and the subsequent physisorption of biomolecules. B) APTES can bind to hydroxyl functional groups of the material surface providing an amine functional group to facilitate covalent bonding with proteins on the other end. That amine group can be activated by different covalent linking agents such as glutaraldehyde. C) UV-graft polymerization with benzophenone and AA produces PAA brushes on the surface. The carboxyl groups of grafted PAA can be covalently linked to ECM proteins *via* carbodiimide-mediated amide formation. D) Positive charged molecules as PDL/PLL are adsorbed by electrostatic interaction on the surface of activated surfaces (negatively charged). Amine groups on PDL can be activated with GA and proteins are covalently immobilised.

dimensionality nor has its effect to counteract cellular forces in 3D cultures been characterised. On the other hand, the adsorption of positively charged molecules such as PDL/PLL on activated surfaces[43–46] and the subsequent activation of amine functional groups with GA for covalent immobilisation to proteins is barely described in PDMS devices.[47] Nevertheless, this approach has not been previously reported on COC/COP surfaces. We were encouraged, therefore, to test several surface treatments (Fig. 2) on COP-MD to form stronger bonds with collagen hydrogel. We hypothesised that improved bonding between collagen hydrogel-embedded fibroblasts and the COP-MD surface should avoid and delay the collapse and detachment caused by fibroblast cell contractility. This would allow the development of *in vitro* models requiring contractile cells.

Experimental

Microdevice fabrication/characteristics

Microfluidic devices (MD) based on cyclic olefin polymers (ZEONOR, Zeon Corporation) were manufactured by injection moulding. The design (Fig. 3A) comprised a central chamber 2000 μm wide and 250 μm deep, flanked by two lateral channels (700 μm wide, 250 μm deep) connected to the central chamber by micropillars. The injected piece (ZEONOR 1420R) was attached to a sheet of COP (ZEONOR 14-100) by biocompatible adhesive (ARseal 8026) and cut out in the area of the central chamber to preserve the whole seeding area in contact with COP (free of adhesive) (Fig. 3B). After applying the surface treatment, the hydrogel seeding solution was injected through an inlet port into the central chamber by manual pipetting. The lateral microchannels remained hydrogel-free and filled with culture medium, simulating blood vessels.

Surface modification and immobilisation strategies

Surface oxidation and physical adsorption. For control devices (Fig. 2A), plasma treatment was carried out on Diener Electronic Plasma-Surface-Technology. COP piece and sheet were placed inside the plasma chamber, and the air was evacuated at 0.4 mbar before filling with oxygen (50%). Glow discharge plasma was created by controlling electrical power at 180 W and a ratio frequency of 13.56 MHz for 60 seconds. Then, the pieces were assembled before sterilising.

Silanisation and covalent bonding. COP silanization protocol (Fig. 2B) was modified from Chuah and coworkers.[48] Briefly, after plasma surface activation, the devices were incubated with 10% APTES (Sigma Aldrich 440140) in water (v/v) for 2 hours at room temperature. APTES solution was removed, and devices were rinsed with distilled water before incubation with 2.5% glutaraldehyde (GA, Sigma Aldrich G6257) for 1 hour at room temperature. Subsequently, the devices were rinsed three times with distilled water to remove GA excess and assembled before sterilising.

Polyacrylic acid photografting and covalent bonding. COP-MD surface was modified by polyacrylic acid photografting (PAA-PG) initiated by UV light. A single-step photografting approach previously described[49,50] was used to graft the COP by irradiation of a solution of monomer containing benzophenone as a photoinitiator (Fig. 2C). More in detail, the treatment solution was composed of initiator benzophenone (0.25% w) (Sigma Aldrich B9300) dissolved in methanol (50% w) (CHEM-LAB CL00.1364.2500), acrylic acid (1% w) (Sigma Aldrich 147230) and distilled water (50% w). Acrylic acid 1% was selected as it led to a hydrophilic surface (WCA = 41.6°) while keeping a good optical transparency. Oxygen was displaced from the treatment solution with argon flow for 3 minutes to avoid inhibition of the reaction by oxygen. COP piece and COP sheet, separately, were placed over a glass with the treatment solution and irradiated with UV-C light (260 nm) for 20 minutes. The grafted surface was rinsed with acetone and water. The pieces of the devices were assembled before protein immobilisation by the crosslinking reaction. Crosslinking of the PAA grafted surface device and ECM proteins was based on Hermanson's protocol.[51] Briefly, 0.15 M EDC (*N*-ethyl-*N*′-(3-dimethylaminopropyl) carbodiimide hydrochloride, Sigma Aldrich 161462) and 0.12 M sulfo-NHS (*N*-hydroxysulfosuccinimide sodium salt solutions, Sigma Aldrich 56485) were dissolved in 0.1 M MES (2-(*N*-morpholino) ethanesulfonic acid hydrate, Sigma Aldrich M8250) (pH 5). EDC and sulfo-NHS solutions were mixed and injected into the central chamber of the device containing acrylic acid moieties for 2 hours at room temperature. After incubation, devices were rinsed with PBS (phosphate-buffered saline) three times.

Physical adsorption and covalent bonding. After plasma surface activation, for PDL hydrobromide treatment, devices were assembled before the following steps (Fig. 2D). A solution of 1 mg mL^{-1} PDL hydrobromide (poly-D-lysine hydrobromide Sigma Aldrich P7886) was injected into the central chamber and incubated for 10 minutes. Once the PDL solution was removed, 0.4% GA was incubated for 30 minutes at room temperature. Next, devices were rinsed three times with PBS to remove GA excess before sterilising.

All devices were sterilised by exposure to a germicidal UV lamp for 30 minutes before cell-embedded collagen hydrogel seeding.

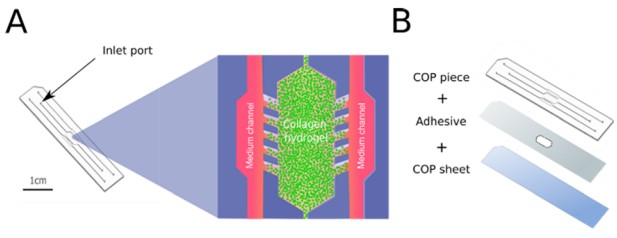

Fig. 3 Microfluidic device appearance and components. (A) Magnified representation of a COP-MD with collagen hydrogel embedded cells (green) confined into the central chamber and culture medium perfused through the two lateral channels creating a gradient of medium. (B) Schematic illustration of the elements integrating the microfluidic device.

3D cell culture

Human cardiac fibroblasts (HCF) (ScienCell) and human dermal fibroblasts (HDF) (Gibco) were grown between passages 3 to 6. HCF were grown in DMEM (Lonza 12-707F) culture medium supplemented with 10% FBS (Sigma F7524) and 2.5 mM L-glutamine (Lonza 17-605c), 1% penicillin/streptomycin (100 μg mL^{-1}) (Lonza DE 17-602E), 10 ng ml^{-1} FGF-2 (Peprotech 100-18B) and 1.5% HEPES (Lonza BE17-737C). HDF were grown in DMEM (Lonza 12-707F) culture media supplemented with 10% FBS (Sigma F7524) and 2.5 mM L-glutamine (Lonza 17-605c), 1% penicillin/streptomycin (100 μg mL^{-1}) (Lonza DE 17-602E), 0.5 ng ml^{-1} FGF-2 (Peprotech 100-18B) and 1.5% HEPES (Lonza BE17-737C). Human glioblastoma cell line U-87 MG was purchased from Sigma Aldrich (Sigma 89081402 lot: 16L024). U-87 MG were grown in high glucose DMEM (Lonza H3BE12-614F) culture medium supplemented with 10% FBS (Sigma F7524) and 2.5 mM L-glutamine (Lonza 17-605c), 1% penicillin/streptomycin (100 μg mL^{-1}) (Lonza DE 17-602E). Media was refreshed every other day, passaging cells every 3–4 days with trypsin/EDTA solution (Lonza, CC-5012). All cell lines were maintained within a humidified TEB-1000 incubator set at 5% CO_2 and 37 °C (EBERS Medical Technology).

Hydrogel mixture for 3D culture into COP-MD was composed of 50% (v/v) of the double desired cell density in growth media and 50% (v/v) collagen matrix. For collagen matrix, either 3.36 mg mL^{-1} (Corning 354236) or 10.98 mg mL^{-1} (Corning 354249) type I rat tail collagen, NaOH 1 N (Sigma 655104) at the proportion of 1 : 40 (v/v of collagen volume) and DMEM 5X (Sigma D5523) at 1 : 5 (v/v of collagen matrix volume) were mixed to get a final collagen density of 1.2 mg mL^{-1} or 4 mg mL^{-1} respectively. Sterile water was added to reach the final collagen matrix volume. The collagen gel matrix was resuspended, homogenised and kept on ice until injection into the devices. The cell suspension at the desired cell density was homogenised with collagen matrix before injecting into the device. COP-MD were pre-warmed at 37 °C for 1 h before cell seeding. Once the cells-collagen gel suspension was confined in the central chamber, devices were turned up and down every 20 seconds for 3 minutes to obtain a homogeneous cell distribution before introducing into the incubator (37 °C, 5% CO_2) for 15 minutes to promote collagen gel polymerisation. Afterwards, the pre-warmed culture medium was perfused through lateral channels and refreshed daily.[52]

Cell tracking and viability assessment

Cells were fluorescently labelled before embedding into the hydrogel by adding 5 μl of lipophilic cell membrane dye Vybrant™ DiO (Invitrogen V22886) per 10^6 cells per mL suspension. Cells were incubated for 15 min, centrifuged and washed three times with a culture medium. Cell viability was assessed by perfusing through the lateral channels with 1 μg mL^{-1} calcein AM (CAM) (Sigma 17783) and 4 μg mL^{-1} propidium iodide (PI) (Sigma P4170). Both stainings were incubated at 37 °C in a humidified chamber with 5% CO_2. Cells cultured into COP-MD were visualised by confocal microscopy (Nikon Ti-E coupled to a C1 modular confocal microscope), at 590/50 nm for Vybrant and CAM and at 650LP nm for PI. Two image types were taken from each device: the top and section view of the central chamber (Fig. 1). To obtain the hydrogel area occupied in the section view, confocal *Z*-stacks were taken at different time points. To acquire the entire height of the chamber, 300 μm thick confocal stacks were performed with images every 10 μm. *Z*-Stacks were performed in at least two regions of each device, evaluating at least three devices per condition. Images were analyzed with Fiji® software[53] for area quantification (ESI† Fig. S2).

The immobilisation efficiency of collagen hydrogel was related to the hydrogel resistance to collapse by cell traction forces and was assessed by measuring the section area occupied (ESI† Fig. S2). Hence, the greater the cell area occupied, the greater the resistance of the hydrogel to collapse and the better hydrogel immobilisation. For cell viability, fluorescence profile intensity across the chamber was quantified by selecting a rectangular region of the central chamber between the medium channels.

Statistical analysis

For statistical analysis, trend lines of transversal area quantification over time were computed using weighted linear regression with an R square ranging from 0.6 to 0.97, from which the slope was estimated. The slope was considered an immobilisation efficiency indicator, so the greater the slope, the greater the gel contraction and, therefore, less hydrogel immobilisation. The significant difference among the conditions was determined by a statistical comparison of the slope pairs using a two-tailed test. Cell viability analysis was determined by a statistical parametric unpaired Student t-test using the statistical software GraphPad Prism 6.01. All experiments were performed at least thrice, and a p-value < 0.05 was considered statistically significant.

Results

Hydrogel immobilisation efficiency evaluation after different COP-MD surface treatments

Three surface treatments in COP devices were assessed prior to immobilisation of fibroblast embedded into 1.2 mg mL^{-1} collagen hydrogels. Thus, collagen I was immobilised to PAA-PG, APTES and PDL pre-treated COP-MD surfaces, taking a plasma-treated surface as control. The most representative changes of hydrogel integrity were monitored and observed in the section view, as the top view does not evidence the whole hydrogel integrity. The section area occupied by green-fluorescent DiO Vybrant™ labelled human cardiac fibroblasts (HCF) (10^7 cells per mL) embedded into collagen (1.2 mg mL^{-1}) hydrogels was monitored over 13 days. Images were acquired until

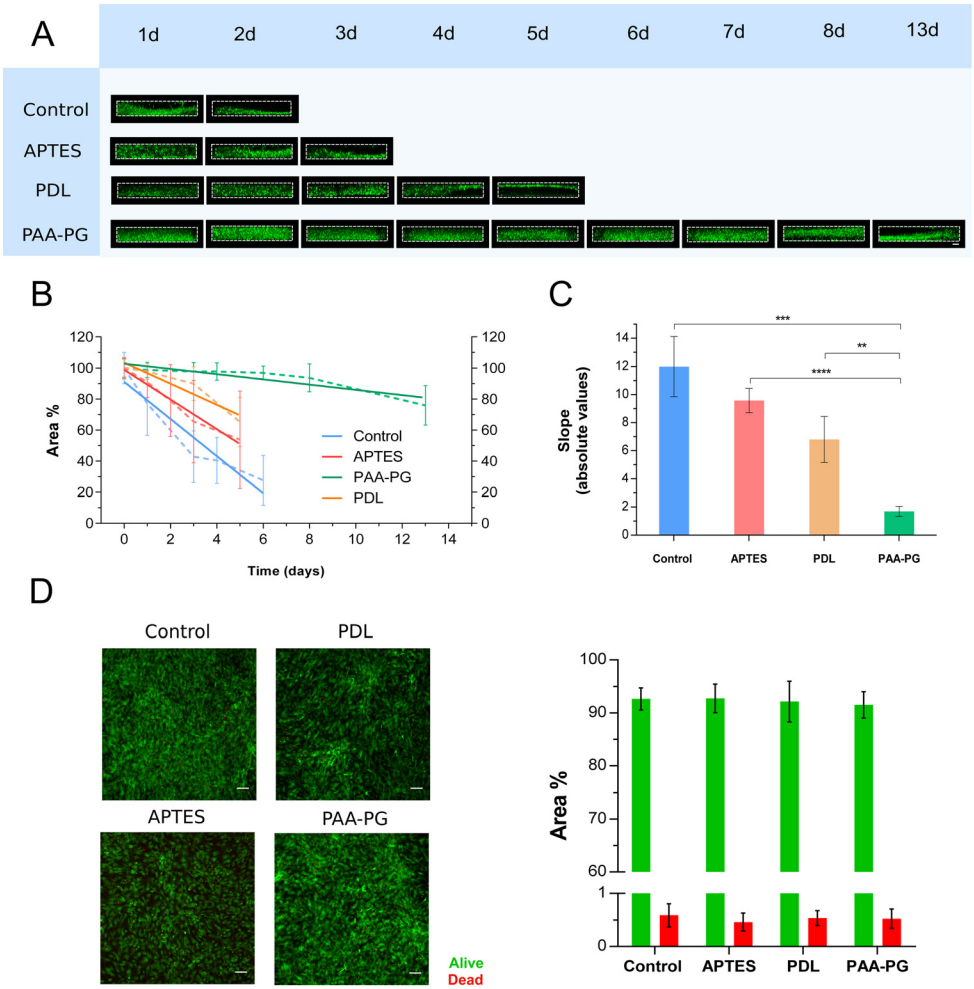

Fig. 4 Culture of HCF (10^7 cells per mL) embedded in 1.2 mg mL^{-1} collagen after device pre-treatments. A) Transversal area evolution overtime of HCF labelled with green-fluorescent DiO Vybrant™ dye. B) Area percentage of HCF embedded collagen hydrogels within the device chamber over time (dashed line) after treatment with different conditions and trend lines (continuous line). C) Statistical comparison among the slopes (absolute values) of trend lines from each condition. D) Micrographs and area percentage of calcein–propidium iodide stained cells from micrographs of collagen embedded HCF within treated devices after 13 days. Error bars SD. Note: **** $p < 0.0001$, *** $p < 0.001$, ** $p < 0.01$, * $p < 0.05$. Error bars SD. Scale bar 100 μm.

collagen hydrogels were completely collapsed (Fig. 4A). Silanization of the surface with APTES displayed a clear hydrogel area reduction after two days, being pronounced on the third day (slope −9.58 ± 0.86) (Fig. 4B). PDL-treated chips reduced their hydrogel area below 90% after four days in culture (slope −6.81 ± 1.64). Finally, PAA-photografting (PAA-PG) treatment showed the longest hydrogel structure preservation, keeping over 90% area after 8 days of culture (slope −1.69 ± 0.36). Then, the first fissures between the device surface and the hydrogel began to be displayed, showing statistically significant differences compared to the control ($p < 0.001$). No tendencies were observed between the top (47.5%) and the bottom (52.5%) when the gels detached from the COP-MD.

Although all studied hydrogels were contracted over time except PAA-PG pre-treatment, we evaluated embedded cell viability after 13 days in all the conditions to determine any possible toxic effect from the chemicals applied on the device surface. Thus, we quantified the cell viability of collagen-embedded HCF and corroborated that all the surface treatments did not significantly affect the cell viability compared with the control (Fig. 4D).

The treatment showing the longest prevention of collagen hydrogel collapse was also tested with other high-contractile cell lines to avoid cell line-specific bias. Thus, PAA-PG was applied to devices seeded with human glioblastoma cell line U-87 MG previously embedded in 1.2 mg mL^{-1} collagen hydrogel. Consistently with the observations of HCF collagen-embedded hydrogels, the treatment displayed significant differences to control, with longer preservation of 3D structure (ESI† Fig. S3). Moreover, PAA-PG treatment exhibited also improved gel resistance to cell forces with collagen-embedded human dermal fibroblasts (HDF) for 3 days, at 2 and 5 × 10^6 cells per mL (ESI† Fig. S4).

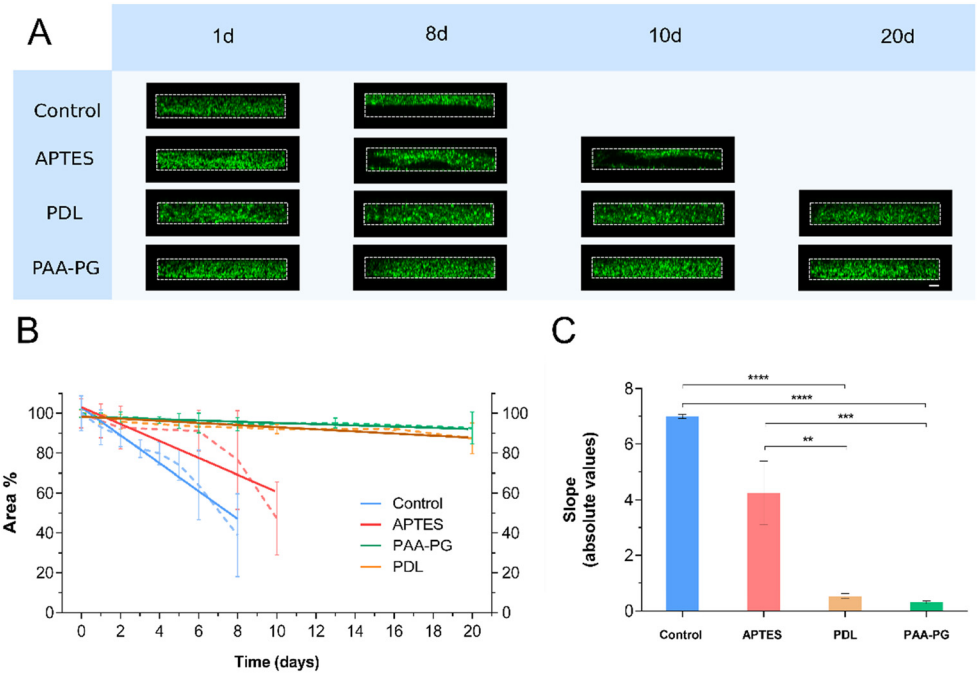

Fig. 5 Culture of HCF (10^7 cells per mL) embedded in 4 mg mL^{-1} collagen after device pre-treatments. (A) Transversal area evolution overtime of HCF labelled with green-fluorescent DiO Vybrant™ dye. (B) Area percentage of HCF occupation of the collagen hydrogel within the device chamber over time (dashed line) and trend lines (continuous line). (C) Statistical comparison among the slopes of trend lines from each condition. Note: **** $p < 0.0001$, *** $p < 0.001$, ** $p < 0.01$ and * $p < 0.05$. Error bars SD. Scale bar 100 μm.

Evaluation of collagen concentration effect on the hydrogel immobilisation efficiency

In order to test the outcomes of the studied surface treatments on collagen contraction within COP-MD at higher collagen concentrations, we tested them with 4 mg mL^{-1} collagen hydrogels (Fig. 5A–C). Thus, the section area of 10^7 HCF embedded in 4 mg mL^{-1} collagen hydrogels within treated COP-MD was monitored over time. In all the studied treatments the shrinkage of 4 mg mL^{-1} collagen hydrogels was delayed compared to that observed in 1.2 mg mL^{-1} collagen hydrogels, still following a similar tendency. This way, PAA-PG treatment displayed the least contracted collagen hydrogels for up to 20 days, followed by PDL-treated devices. Furthermore, in contrast to 1.2 mg mL^{-1} assays, PDL treatment kept uncontracted collagen hydrogels nearly as long as PAA-PG. This behaviour in PDL-treated devices was reflected by the slope of the trend lines from the cell area percentage occupied within the hydrogel in the device chamber, showing statistically significant differences to control and comparable to PAA-PG ($p < 0.0001$). In fact, the cell area percentage occupied in PDL-treated microdevices kept above 90% until day 20 of culture, similar to PAA-PG. Still, it decreased slightly at this point, with some gels detaching from the surface of the microdevice. Finally, silanization with APTES (slope −4.245 ± 1.146) did not show differences to control as described with 1.2 mg mL^{-1} collagen results, preserving cell area percentage occupied within devices above 90% up to the 6 day of culture.

To better understand the surface distribution of the treatment and surface attachment forces to collagen I, complementary assays with shear stress were performed (ESI† Fig. S5). The surface of rectangular COP-channels was treated and coated with fluorescently-labelled collagen I.

The distribution of functional groups, responsible for protein immobilisation, was indirectly quantified by analysing the collagen bonded to the COP surface for each condition before applying shear stress (0 dyn cm^{-2}). Contrary to other types of proteins (ESI† Fig. S6A) collagen distributed in aggregates (ESI† Fig. S5A). This is probably caused by the variability in their size and structural properties. Regarding the quantity of immobilised collagen, significant differences were only observed between control and PDL surfaces (ESI† Fig. S5B).

To compare the adhesion forces of the collagen to the differently treated COP surfaces, collagen-coated channels were exposed to increasing shear stress forces (0.15, 25 and 150 dyn cm^{-2}). Fluorescence microscopy revealed that the collagen presence varied before and after shear stress application. Consistently with 3D cell embedded assays, in control condition (plasma) collagen was almost completely detached from the surface after applying the lowest shear stress (0.15 dyn cm^{-2}). Indeed, the remaining quantity of collagen was 12.5% of the initial state. In the other treated surfaces (APTES, PDL and PAA-PG) collagen quantity slightly decreased when shear forces of either 0.15 or 25 dyn cm^{-2} were applied (ESI† Fig. S5B). Lastly, more pronounced changes were observed with the maximum shear stress (150

dyn cm^{-2}). For the APTES surface, the collagen quantity was reduced to approximately 28% of the initial state. In turn, for the PDL and PAA-PG channels, this parameter was reduced to 61% and 75%, respectively. These results agree with the previously described observations for collagen hydrogel resistance to cell contraction (Fig. 4 and 5).

PAA-PG was tested with other types of extracellular matrix proteins with a key role in cell adhesion such as fibronectin and laminin (ESI† Fig. S6). Plasma control and PAA-PG channels were coated with fluorescently-labelled fibronectin and laminin and exposed to 150 dyn cm^{-2}. Although the initial distribution was very homogeneous for both laminin and fibronectin, the fluorescence intensity showed different values (ESI† Fig. S6B). Fibronectin control channels displayed a minor intensity than PAA-PG channels. Though in PAA-PG channels fluorescence intensity decreased after flow, it still maintained a higher intensity than control in static conditions. On the other hand, the intensity of laminin was greater in PAA-PG channels compared with the control ones before flow. Nevertheless, despite both conditions showed protein detachment, the intensity levels of control channels were better maintained than PAA-PG ones. These results suggested an improved immobilisation of fibronectin to PAA-PG surfaces in comparison with the laminin.

Evaluation of PAA-PG immobilisation technique for the *in vitro* simulation of the necrotic core formation

The presence of fibroblasts in co-cultures of different cell types is often needed to create more biomimetic *in vitro* models. However, fibroblasts are one of the main cell types affecting 3D hydrogel integrity. Moreover, some experiments require high cell densities inside the gel as the self-induced ischaemia models,[52,54] in which the fibroblast role is extremely relevant. Thus, we tested if PAA-PG pre-treatment could overcome this technical obstacle, focusing on a necrotic core model with human cardiac fibroblasts in 1.2 mg mL^{-1} collagen hydrogels.

First, we assessed the influence of the HCF cell density on contracting the hydrogel. Low-dense cultures (10^6 cells per mL) of HCF did not produce collagen hydrogel contraction when the device was not treated (control) (Fig. 6A). However, the hydrogel contraction was observed after 3 days with 5×10^6 cells per mL and only 24 hours with higher densities (10^7 and 2×10^7 cells per mL) (Fig. 6B). The PAA-PG pre-treated microdevices improved performance significantly, successfully preserving the hydrogel structure after 3 days in culture at all the densities studied (Fig. 6C). Vybrant DiO fluorescence intensity and cell morphology differences were observed in the central area of the culture chamber in the highest HCF concentration hydrogels (10^7 and 2×10^7 cells per mL). Fibroblasts located closer to the medium channels were more fluorescent and spread. At the same time, cell morphology in the central area was rounded and fluorescence intensity lower, suggesting cell death (Fig. 6D–H, S7 and ESI† video). Cell viability staining after 48 hours showed rounded central cells as dead and membrane compromised cells, generating a necrotic core in the innermost hydrogel region. The necrotic core generated after 48 hours by a density of 10^7 cells per mL occupied 500–600 μm of the central chamber (Fig. 6I). A higher cell density of 2×10^7 cells per mL provided a larger necrotic core, up to 1500 μm (Fig. 6J).

Accordingly, the pre-treatment with PAA-PG allows the generation of a necrotic core with fibroblasts embedded in collagen hydrogel, which was impossible without collagen hydrogel immobilisation (Fig. 6B and C). The effectiveness of PAA-PG was even more evident when studying the human glioblastoma U87-MG cell line. Thus, comparing non-treated COP-MD with PAA-PG treated, we were able to prolong the culture of 4×10^7 U87-MG cells per mL embedded in collagen from 4 hours to 9 days. Moreover, a necrotic core was preserved 9 days after cell seeding (ESI† Fig. S8).

Discussion

Fibroblast concentration and ECM stiffness are parameters that influence physiological and non-physiological phenomena. For example, in fibrosis and wound healing processes, an acute injury triggers a cascade of events that lead to fibroblast migration and proliferation. These fibroblasts produce large amounts of ECM proteins, including collagen type I and III, fibronectin and hyaluronic acid, leading to increased mechanical tensions in combination with other chemical stimuli that induce transdifferentiation of fibroblasts into myofibroblasts. Myofibroblasts are characterised by the ability to exert strong contractile forces on the ECM, and produce fibrillar collagen bundles that stiffen the tissue. Similarly, tumours have been described as wounds that fail to heal, where the fibroblasts play an important role by producing and depositing ECM that enhances stiffness and strain.[2,55] All these aspects make the *in vitro* biomimetic recreation of these processes, in which fibroblasts are involved, a matter of crucial importance. However, the generation of models based on microfluidic devices has been very limited by the contractile capacity of fibroblasts on the hydrogel structure in which they are embedded. These contractions cause gel collapse, altering the organisation and distribution of cells in microfluidic devices. Therefore, the need arises to develop surface treatments for the chip materials to avoid hydrogel collapse. In this work, several protein immobilisation methods have been compared in COP-MD.

From the different methodologies reported (low-pressure plasma, oxygen plasma, UV/ozone, photografting of PEGMA/PEtOx, permanent PVA coating and dynamic HEC coating), oxygen plasma appears as a very effective technique in terms of reducing hydrophobicity and generating functional groups in COP/COC substrates.[56,57] However, the oxygen plasma effect depends on the polymer type. The reduction of the WCA is an indicator of the increase in surface energy due to the introduction of polar groups on the surface of the

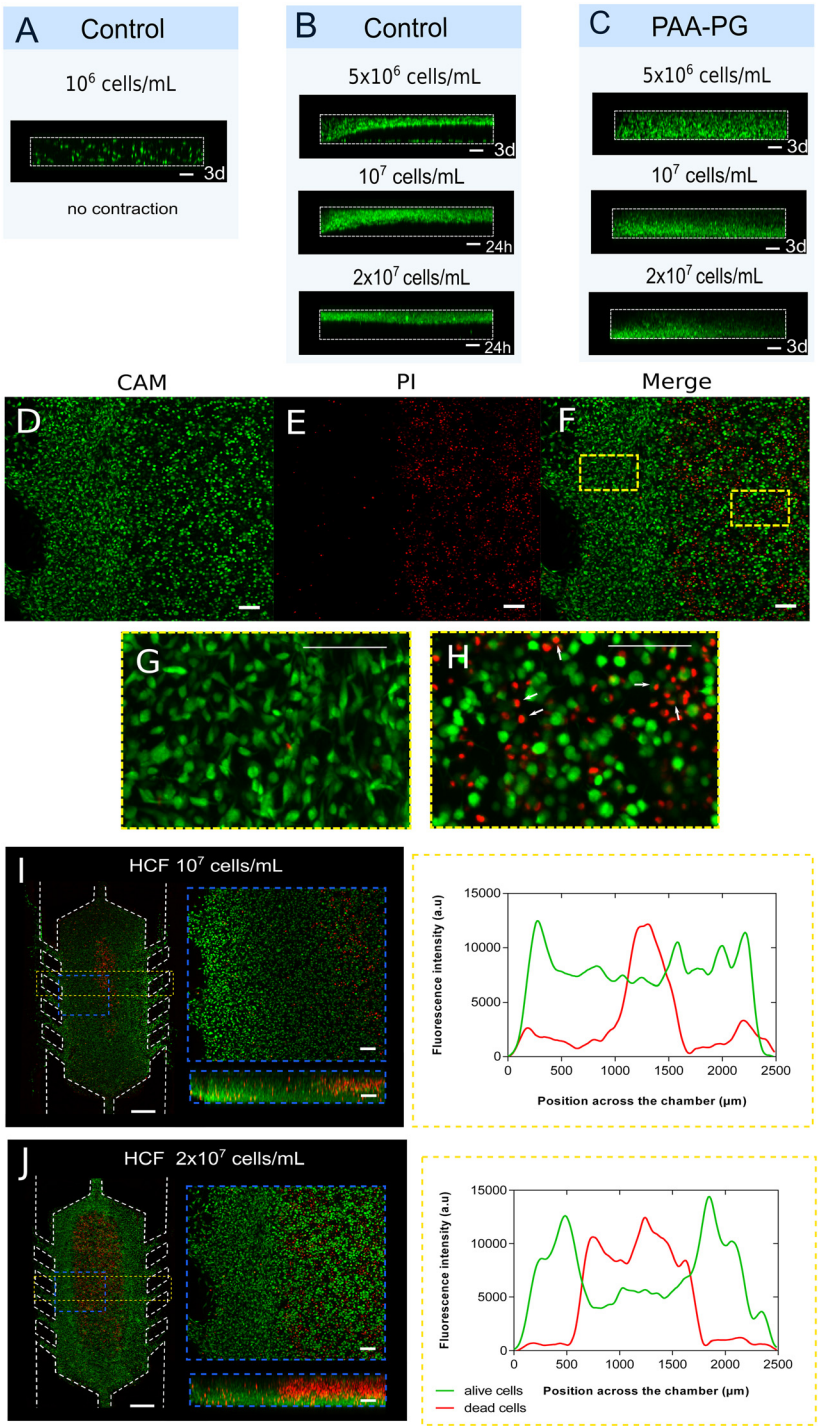

Fig. 6 HCF 3D culture for necrotic core formation in PAA-PG treated devices. (A) Green labelled (DiO) HCF at 10^6 cells per mL in collagen (1.2 mg mL^{-1}) hydrogel within non-treated microdevice after 3 days. Cardiac fibroblasts at 5×10^6, 10^7 and 2×10^7 cells per mL section view within non-treated (B) and PAA-PG treated (C) COP-MD. 2×10^7 HCF mL^{-1} after 48 hours culture labelled with (D) calcein (CAM) and (E) propidium iodide (PI) viability stain presented two different areas, being the area on the left densely populated whereas that the right area displayed less cells, separated from each other. PI binds to nucleic acids of dead cells, mainly grouped in the center of the chamber (right area in E), where gases and nutrients levels decrease. Merging CAM and PI micrographs (F) revealed the coincidence of the right area with the predominance of dead cells. Magnifying the image in the region closer to the medium channels (left in F) cells exhibited a spindle like form (G) while in the central region of the chamber (right in F) cells showed a rounded morphology (H). In addition, in the right area (marked with white arrows in H) red stained nuclei disclosed inside green fluorescent cells, suggesting that these cells have a compromised membrane. Top and section view (blue bordered regions) of alive/dead fibroblasts of 10^7 (I) and 2×10^7 (J) HCF mL^{-1} at 48 hours after CAM/PI staining. The graphs show quantification of CAM (green) and PI (red) fluorescence intensity profile along the chamber device (yellow bordered regions). Scale bar 100 μm except in (I) and (J) left image of the whole device where scale bar is 500 μm.

polymer. For example, differences in the ethylene/norbornene content in COC (Topas®) are described to affect the WCA. An increased norbornene content lead to a lower WCA and more hydrophilic surface after oxygen plasma-activation.[58] Haq *et al.*,[59] applied a corona treatment to polycarbonate, COC and COP surfaces, obtaining a reduction from 80° to 38°, 96° to 39° and 93° to 27°, respectively. The WCA reduction was related to the increment of oxygen to carbon ratio in C–O, COH, COOH and C═O forms. These results suggest a different surface activation of COP and COC under the same treatment conditions. In cell culture applications,[60] COP (Zeonex®) and COC (Topas®) air plasma-treated substrates were seeded with HeLa cells (cervix carcinoma cells). COP was described as a suitable substrate for cell culture while COC did not provide an appropriate chemistry for cells. Despite COP and COC are chemically related, spectroscopy analysis showed different spectra. Authors suggested the presence of non-specified additives in the polymers to explain the differences observed in the cell culture studies.

Among all the treatments studied in this work, the physisorption treatment (control) has shown the worst response to counter hydrogel contraction. This was expected because the intramolecular forces involved are weak and unstable, needing additional treatments to enhance protein attachment.[30,61,62] The short stability of plasma oxidation has been widely reported in both PDMS and COC materials[36,63] extensive also to their ability to adsorb molecules on their surface. For example, AFM height images from collagen coating physically adsorbed onto PDMS after oxygen plasma treatment show lower stability after incubation in a growth medium for five days than stable covalent coating based on an aminosilane chemistry.[64] Moreover, according to published studies of monolayer cultures on collagen coating[65,66] and collagen-embedded cells[46] within microfluidic devices, it seems that the physical adsorption of collagen I does not represent an ideal host surface for the long-term culture of cells. Although this lack of stability can be attributed to cell activity and homeostasis, the adsorbed collagen can also be exchanged by other proteins from the cell culture medium, known as the Vroman effect, making immobilisation less stable and resistant to cell remodelling.[66]

Positively charged molecules (PDL/PLL) have been commonly used as a cell adhesion molecule to enhance cell attachment, adhesion and differentiation of many cell types.[67] Some works describe the immobilisation of PDL through APTES[67] or Pluronic F127[68] to stabilise and improve neuron adhesion with in long-term cultures. Direct PDL adsorption on plasma-activated surfaces prevents shrinkage and detachment of collagen hydrogel from PDMS channels allowing capillary morphogenesis.[43,46] Treatment with NH_2 ended chemicals such as poly(ethyleneimine) (PEI), pol-y(allylamine hydrochloride) (PAH), hexamethylenediamine (HMDA) and 1,3-diaminopropane (DAP) has been reported in PMMA[69] and porous silicon substrates[70] for antibody immobilisation. Recently, substrate amination with PLL to immobilise ECM protein has been used in PDMS devices to promote better bonding in cell culture applications.[47,71] To the authors' knowledge, this is the first time that amination with PDL is used for collagen immobilisation on COP surfaces for 3D culture applications. In this work, heterogeneous results were observed in combined physisorption and covalent bond treatment with PDL. Followed by GA activation, PDL amino groups covalently crosslink with collagen amino groups. Thus, PDL treatment delayed the hydrogel contraction, maintaining the cell area occupied over 90% up to 3 days with 1.2 mg mL^{-1} collagen hydrogels, which was significantly prolonged with 4 mg mL^{-1} collagen hydrogels. Hence, our results point to PDL treatment as the second-best immobilisation technique after PAA-PG.

Grafting is a widely used technique for modifying the surface chemistry with polymer brushes for further modification in both PDMS and COC/COP. It allows a stable hydrophilic surface, can provide stable biomolecule attachment and provides biocompatibility with the possibility of patterning enclosed microchannels.[27] Covalent attachment of graft chains onto a polymer surface offers stable surfaces in contrast to the physical coatings which can be delaminated.[41] In microfluidics, the applications for grafted substrates are principally: reducing protein adsorption and platelet adhesion, providing anti-fouling properties, and immobilising antibodies and biomolecules.[72] Wang *et al.*,[31] successfully photografted PAA onto PDMS substrates and subsequently immobilised a mixture of ethylenediamine, chitosan, PLL and RGD peptides to promote cell attachment and growth in the modified regions. Similarly, in COP/COC substrates photografting has been predominantly used to generate microfluidic sensors by bioanalytical probes immobilisation,[42,73] the reduction of nonspecific adsorption of plasma proteins or BSA[74] and cell adhesion.[40] Remarkably, photografting has not been reported to immobilise collagen either to avoid hydrogel collapse or to improve coating efficiency in COP-MD. In this work, we demonstrate that COP-MD previously treated by PAA-PG reached the longest fibroblast 3D culture, preserving hydrogel structure without collapsing at either 1.2 or 4 mg mL^{-1} collagen concentration after 8 days. Comparing the effect of PAA-PG and PDL immobilisation treatments, PDL-treated chips did not preserve the 3D structure as long as UV-photografting, possibly due to the chemical strength differences between both treatments. In fact, while PAA-PG presents double covalent bonding between COP-PAA and PAA–collagen, PDL is physisorbed onto the COP surface by electrostatic interaction and covalently bonded to collagen through the amino groups exposed by GA linked to PDL.

We also studied immobilisation by silanization with APTES, since this technique is widely applied for antibody immobilisation for immunoassays diagnosis in materials such as COP or COC.[36–38] However, although ECM proteins immobilisation with APTES in PDMS microfluidic devices is successfully reported in cell sheet cultures (enhancing cell adhesion[66,75] under shear stress conditions[64] or for cell stretching applications[76]), there are no studies in 3D culture

within microfluidic devices. Interestingly, although PAA-PG and APTES treatments are supposed to establish stable covalent linkages between proteins and chemically modified COP surface, only PAA-PG showed significant outcomes. APTES was shown as a non-appropriate immobilisation technique for collagen I-based hydrogels in COP-MD under the conditions applied in this work. Further investigation exploring extended surface activation times applied to 3D culture must be done.

Increasing collagen hydrogel concentration induced a delay in contraction behaviour. As reported, higher collagen concentration gels exhibit minor contraction than less concentrated ones.[77] Consequently, the contraction tendency between 1.2 mg mL^{-1} and 4 mg mL^{-1} collagen hydrogels was very similar, so the efficacy of the treatments was almost equal. Thus, collagen hydrogel concentration directly affects the time required for cell contraction, delaying the phenomenon, but not avoiding it. Nevertheless, increasing collagen hydrogel concentration modifies mechanical properties such as elastic modulus, pore radius or permeability[78] inducing changes in cell behaviour.[77] Therefore, this strategy is not always close to physiological microenvironment stiffness.

Cancer cell spheroids (also known as multicellular tumour spheroids MCTS) are a successful *in vitro* model to mimic cell-to-cell interactions and tumour/ischaemia models. The core of solid tumours is highly hypoxic due to poor blood circulation. Moreover, hypoxia is considered to contribute to drug resistance,[79] being one of the major hallmarks of solid tumours and a requirement for 3D tumour culture models. Due to the limited diffusion within spheroids, biochemical gradients are created (oxygen, nutrients, growth factors, signalling molecules and molecular waste).[80] Nevertheless, microscopic imaging of large spheroids (>150 μm) and organoids is extremely challenging or requires expensive equipment due to poor light and label penetration, and attenuation of the fluorescent signal by light scattering.[81,82] On the other hand, scaffolds based on hydrogels provide extracellular support, mimicking the biochemical and mechanical properties of ECM, allowing for cell–ECM interactions,[10] cell growth and migration. Their tuneable porosity allows the diffusion of oxygen, nutrients and drugs to reach the cells while facilitating the waste removal. Combined with COP-MD, hydrogels permit the generation of ischaemia and necrotic core models due to the gas impermeability of COP, with the generation of nutrients and gas gradients inside the central chamber.[52,54] However, the power of this type of ischaemia-on-chip model lies not only in the capacity to control the gas concentration inside the device (material properties) but also in the preservation of the three-dimensionality of the culture within the chamber. When including cells with contractile capacity within the hydrogel, its structure may be compromised and, therefore, the preservation of three-dimensionality and gradient generation. This phenomenon encouraged us to study PAA-PG surface functionalisation to validate an ischaemia-on-chip model with contractile cells. This treatment demonstrated long-term 3D culture, preserving collagen hydrogel structure. We were able to generate oxygen and nutrient gradients that led to the formation of necrotic cores. In fact, different necrotic core sizes were developed depending on initial HCF density seeding. PAA-PG also permitted a glioblastoma necrotic formation with U87-MG expressing high contractility capacity. The dimensions of the necrotic cores generated in this work are conditioned by the nature of the extracellular matrix (type of protein, concentration, porosity), the density and cell type (cell requirements and metabolism) and the characteristics of the device (design and dimensions). The latter can affect the diffusion of the culture medium. Relying on the size of the medium channels, the volume of culture medium available will vary. Another relevant feature is the presence of microchannels connecting the central chamber and the medium channels. These structures limit the area of contact and diffusion. Likewise, the culture medium flow rate constitutes an important factor to control the medium diffusion speed through the hydrogel.

Not only fibroblast-like cell types do manifest contractility events, but also endothelial cells retract hydrogels away from the walls of microfluidic devices in long-term experiments for *in vitro* angiogenesis.[46] Hence, our approach could open the door to the application of the described surface treatments to other models. Moreover, adapting spheroids assays to hydrogel-embedded culture would allow easy real-time monitoring of ischaemia events and other applications such as drug testing and immunotherapy. This constitutes a basis for the development of closer patho-physiological and relevant co-culture models of angiogenesis, wound healing, tumour microenvironment and ischaemia within COP-MD.

Conclusions

We have characterised different protein immobilisation methods for 3D cell culture in COP microfluidic devices showing that collagen hydrogel contraction can be delayed when cultured with highly contractile cells such as fibroblasts. A combination of physisorption and covalent bonding methods for collagen immobilisation using PDL can be applied for long-term cultures in 3D hydrogels. However, their effectiveness on 3D collagen structure maintenance must be determined in advance for each condition (hydrogel concentration, experiment time) or cell type. In this work, we present PAA-PG as the most effective immobilisation method that allows long-term culture at high cell densities of contractile cell types such as fibroblasts. Moreover, PAA-PG allows the generation of gradients and necrotic core within COP-MD cultured with a high fibroblast density. The implementation of PAA-PG treatment to COP-MD opens new possibilities for *in vitro* model generation where collagen hydrogel structure preservation is required, such as ischaemia or tumour microenvironment.

Author contributions

SGL: conceptualization, formal analysis, investigation, methodology, visualization, writing – original draft, writing – review & editing. TR: formal analysis, investigation, methodology, visualization, writing – review & editing. JC: formal analysis, supervision, writing – original draft, writing – review & editing. MLV: investigation, methodology. RM: conceptualization, funding acquisition, project administration, supervision, writing – review & editing. CSS: conceptualization, funding acquisition, project administration, supervision, writing – review & editing. IO: conceptualization, funding acquisition, project administration, supervision, writing – review & editing.

Conflicts of interest

IO and RM are promoters for BeOnChip S.L. (Zaragoza, Spain). SGL is developing her PhD in collaboration with BeOnChip S.L. BeOnChip S.L. does not benefit or take part in any economic decisions of this work. TR, JC, MLV and CSS have no conflicts to declare.

Acknowledgements

SGL was funded by a Spanish MINECO fellowship (DI-17-09585). TR studentship was supported by Instituto de Salud Carlos III (i – PFIS IFI16/00050). This work was funded by CDTI (SNEO-20181019), Spanish Government "Ministerio de Ciencia, Innovación y Universidades (MCIU)" through AEI/FEDER(UE) project PID2020-118485RB-I00; "Ministerio de Asuntos Económicos y Transformación Digital – Agencia Estatal de Investigación" through PID2020-118485RB-I00 and PID2021-126051OB-C41 projects. Government of Aragon project LMP221_21, FEDER (EU); through the "Fondo Social Europeo" (DGA T62_20R, E15_20R and E47_20R). This project has received funding from the European Union's Horizon 2020 research and innovation programme under grant agreement No. 829010 (PRIME) and from H2020-MSCA-RISE-2017 programme under grant agreement No. 778354 (CISTEM); and also from the Key Digital Technologies Joint Undertaking with 876190. Authors would like to acknowledge the use of Servicio General de Apoyo a la Investigación-SAI, Universidad de Zaragoza. The authors want to especially thank Arantxa González for the donation of human cardiac fibroblasts and Jacobo Ayensa for statistical advisory.

Notes and references

1 M. W. Tibbitt and K. S. Anseth, *Biotechnol. Bioeng.*, 2009, **103**, 655–663.
2 C. Frantz, K. M. Stewart and V. M. Weaver, *J. Cell Sci.*, 2010, **123**, 4195–4200.
3 W. Tan and T. A. Desai, *Biomed. Microdevices*, 2003, **5**, 235–244.
4 J. Padron, *Crit. Rev. Oncol. Hematol.*, 2000, **36**, 141–157.
5 R. M. Sutherland, *Science*, 1988, **240**, 177–240.
6 A. Berglund, B. Glimelius, J. Bergh, O. Brodin, M.-L. Fjällskog, H. Hagberg, A. von Heideman, R. Larsson, B. Tholander, M. de la Torre, G. Aström, K. Oberg, G. Parö and P. Nygren, *Med. Oncol.*, 2002, **19**, 151–159.
7 Y. Fang and R. M. Eglen, *SLAS Discovery*, 2017, **22**, 456–472.
8 S. Breslin and L. O'Driscoll, *Drug Discovery Today*, 2013, **18**, 240–249.
9 K. E. Sung, G. Su, C. Pehlke, S. M. Trier, K. W. Eliceiri, P. J. Keely, A. Friedl and D. J. Beebe, *Biomaterials*, 2009, **30**, 4833–4841.
10 S. R. Caliari and J. A. Burdick, *Nat. Methods*, 2016, **13**, 405–414.
11 V. van Duinen, S. J. Trietsch, J. Joore, P. Vulto and T. Hankemeier, *Curr. Opin. Biotechnol.*, 2015, **35**, 118–126.
12 W. J. Polacheck, R. Li, S. G. M. Uzel and R. D. Kamm, *Lab Chip*, 2013, **13**, 2252–2267.
13 A. Boussommier-Calleja, R. Li, M. B. Chen, S. C. Wong and R. D. Kamm, *Trends Cancer*, 2016, **2**, 6–19.
14 A. M. Malek and S. Izumo, *J. Cell Sci.*, 1996, **109**, 713–726.
15 N. E. Ajami, S. Gupta, M. R. Maurya, P. Nguyen, J. Y.-S. Li, J. Y.-J. Shyy, Z. Chen, S. Chien and S. Subramaniam, *Proc. Natl. Acad. Sci. U. S. A.*, 2017, **114**, 201707517.
16 B. M. Baker, B. Trappmann, S. C. Stapleton, E. Toro and C. S. Chen, *Lab Chip*, 2013, **13**, 3246–3252.
17 P. Fernandez and A. R. Bausch, *Integr. Biol.*, 2009, **1**, 252–259.
18 J. A. Hubbell, *Nat. Mater.*, 2008, **7**, 1–2.
19 M. Ahearne, *Interface Focus*, 2014, **4**, 20130038.
20 B. M. Gillette, J. A. Jensen, B. Tang, G. J. Yang, A. Bazargan-Lari, M. Zhong and S. K. Sia, *Nat. Mater.*, 2008, **7**, 636–640.
21 F. Grinnell, *Trends Cell Biol.*, 2000, **10**, 362–365.
22 M. E. Smithmyer, L. A. Sawicki and A. M. Kloxin, *Biomater. Sci.*, 2014, **2**, 634–650.
23 E. Bell, B. Ivarsson and C. Merrill, *Proc. Natl. Acad. Sci. U. S. A.*, 1979, **76**, 1274–1278.
24 M. Yamato, E. Adachi, K. Yamamoto and T. Hayashi, *J. Biochem.*, 1995, **117**, 940–946.
25 S. I. Montanez-Sauri, K. E. Sung, J. P. Puccinelli, C. Pehlke and D. J. Beebe, *J. Lab. Autom.*, 2011, **16**, 171–185.
26 D. Kim and A. E. Herr, *Biomicrofluidics*, 2013, **7**, 1–47.
27 A. Shakeri, N. A. Jarad, S. Khan and T. F. Didar, *Anal. Chim. Acta*, 2022, **1209**, 339283.
28 C. Cha, E. Antoniadou, M. Lee, J. H. Jeong, W. W. Ahmed, T. A. Saif, S. A. Boppart and H. Kong, *Angew. Chem., Int. Ed.*, 2013, **52**, 6949–6952.
29 Z. Yue, X. Liu, P. J. Molino and G. G. Wallace, *Biomaterials*, 2011, **32**, 4714–4724.
30 A. Gokaltun, M. L. Yarmush, A. Asatekin and O. B. Usta, *Technology*, 2017, **05**, 1–12.
31 Y. Wang, H. H. Lai, M. Bachman, C. E. Sims, G. P. Li and N. L. Allbritton, *Anal. Chem.*, 2005, **77**, 7539–7546.
32 W. J. Polacheck, L. Kutys, J. Yang, J. Eyckmans, Y. Wu, H. Vasavada, K. K. Hirschi and C. S. Chen, *Nature*, 2017, **552**, 258–262.
33 W. J. Polacheck, M. L. Kutys, J. B. Tefft and C. S. Chen, *Nat. Protoc.*, 2019, **14**, 1425–1454.

34 W. S. R. Lago, C. Aymes-Chodur, A. P. Ahoussou and N. Yagoubi, *J. Mater. Sci.*, 2017, **52**, 6879–6904.
35 P. S. Nunes, P. D. Ohlsson, O. Ordeig and J. P. Kutter, *Microfluid. Nanofluid.*, 2010, **9**, 145–161.
36 J. Raj, G. Herzog, M. Manning, C. Volcke, B. D. MacCraith, S. Ballantyne, M. Thompson and D. W. M. Arrigan, *Biosens. Bioelectron.*, 2009, **24**, 2654–2658.
37 C. Jönsson, M. Aronsson, G. Rundström, C. Pettersson, I. Mendel-Hartvig, J. Bakker, E. Martinsson, B. Liedberg, B. MacCraith, O. Öhman and J. Melin, *Lab Chip*, 2008, **8**, 1191–1197.
38 D. Sung, D. H. Shin and S. Jon, *Biosens. Bioelectron.*, 2011, **26**, 3967–3972.
39 Y. Qi, Y. Wang, C. Chen, C. Zhao, Y. Ma and W. Yang, *ACS Appl. Bio Mater.*, 2020, **3**, 3203–3209.
40 R. K. Jena and C. Y. Yue, *Biomicrofluidics*, 2012, **6**, 1–12.
41 S. Roy, C. Y. Yue, S. S. Venkatraman and L. L. Ma, *Sens. Actuators, B*, 2013, **178**, 86–95.
42 F. Luna-Vera, J. D. Ferguson and J. C. Alvarez, *Anal. Chem.*, 2011, **83**, 2012–2019.
43 Y. Shin, S. Han, J. S. Jeon, K. Yamamoto, I. K. Zervantonakis, R. Sudo, R. D. Kamm and S. Chung, *Nat. Protoc.*, 2012, **7**, 1247–1259.
44 L. Wang, B. Sun, K. S. Ziemer, G. A. Barabino and R. L. Carrier, *J. Biomed. Mater. Res., Part A*, 2010, **93**, 1260–1271.
45 Y. Shin, H. Kim, S. Han, J. Won, H. E. Jeong, E. S. Lee, R. D. Kamm, J. H. Kim and S. Chung, *Adv. Healthcare Mater.*, 2013, **2**, 790–794.
46 S. Chung, R. Sudo, I. K. Zervantonakis, T. Rimchala and R. D. Kamm, *Adv. Mater.*, 2009, **21**, 4863–4867.
47 A. Chhabra, H. H. G. Song, K. A. Grzelak, W. J. Polacheck, H. E. Fleming, C. S. Chen and S. N. Bhatia, *Proc. Natl. Acad. Sci. U. S. A.*, 2022, **119**, 1–11.
48 Y. J. Chuah, Y. T. Koh, K. Lim, N. V. Menon, Y. Wu and Y. Kang, *Sci. Rep.*, 2015, **5**, 1–12.
49 T. B. Stachowiak, F. Svec and J. M. J. Fréchet, *Chem. Mater.*, 2006, **18**, 5950–5957.
50 T. Rohr, D. F. Ogletree, F. Svec and J. M. J. Frøchet, *Adv. Funct. Mater.*, 2003, **13**, 264–270.
51 G. T. Hermanson, *Bioconjugate techniques*, 2013.
52 J. M. Ayuso, M. Virumbrales-Muñoz, A. Lacueva, P. M. Lanuza, E. Checa-Chavarria, P. Botella, E. Fernández, M. Doblare, S. J. Allison, R. M. Phillips, J. Pardo, L. J. Fernandez and I. Ochoa, *Sci. Rep.*, 2016, **6**, 1–16.
53 J. Schindelin, I. Arganda-Carreras, E. Frise, V. Kaynig, M. Longair, T. Pietzsch, S. Preibisch, C. Rueden, S. Saalfeld, B. Schmid, J. Y. Tinevez, D. J. White, V. Hartenstein, K. Eliceiri, P. Tomancak and A. Cardona, *Nat. Methods*, 2012, **9**, 676–682.
54 M. Virumbrales-Muñoz, J. M. Ayuso, A. Lacueva, T. Randelovic, M. K. Livingston, D. J. Beebe, S. Oliván, D. Pereboom, M. Doblare, L. Fernández and I. Ochoa, *Sci. Rep.*, 2019, **9**, 1–14.
55 P. Pakshir and B. Hinz, *Matrix Biol.*, 2018, **68–69**, 81–93.
56 I. Beaulieu, M. Geissler and J. Mauzeroll, *Langmuir*, 2009, **25**, 7169–7176.
57 P. Ganser, C. Baum, D. Chargin, A. F. Sauer-Budge and A. Sharon, *Biomed. Microdevices*, 2018, **20**, 24.
58 C. E. O'Neil, S. Taylor, K. Ratnayake, S. Pullagurla, V. Singh and S. A. Soper, *Analyst*, 2016, **141**, 6521–6532.
59 A. U. Haq, A. Boyd, J. Acheson, J. McLaughlin and B. J. Meenan, *Surf. Coat. Technol.*, 2019, **362**, 185–190.
60 Å. Ö. B. Johansson, A. Larsson and A. Ocklind, *J. Appl. Polym. Sci.*, 2002, **86**, 2618–2625.
61 A. J. S. Ribeiro, A. K. Denisin, R. E. Wilson and B. L. Pruitt, *Methods*, 2016, **94**, 51–64.
62 A. Oláh, H. Hillborg and G. J. Vancso, *Appl. Surf. Sci.*, 2005, **239**, 410–423.
63 S. J. Hwang, M. C. Tseng, J. R. Shu and H. Her Yu, *Surf. Coat. Technol.*, 2008, **202**, 3669–3674.
64 A. Siddique, T. Meckel, R. W. Stark and S. Narayan, *Colloids Surf., B*, 2017, **150**, 456–464.
65 Y. J. Chuah, S. Kuddannaya, M. H. A. Lee, Y. Zhang and Y. Kang, *Biomater. Sci.*, 2015, **3**, 383–390.
66 Z. Qian, D. Ross, W. Jia, Q. Xing and F. Zhao, *Bioact. Mater.*, 2018, **3**, 167–173.
67 Y. H. Kim, N. S. Baek, Y. H. Han, M. A. Chung and S. D. Jung, *J. Neurosci. Methods*, 2011, **202**, 38–44.
68 W. Liu, K. Han, M. Sun and J. Wang, *Lab Chip*, 2019, **19**, 3162–3167.
69 Y. Bai, C. G. Koh, M. Boreman, Y. J. Juang, I. C. Tang, L. J. Lee and S. T. Yang, *Langmuir*, 2006, **22**, 9458–9467.
70 J. Yakovleva, R. Davidsson, A. Lobanova, M. Bengtsson, S. Eremin, T. Laurell and J. Emnéus, *Anal. Chem.*, 2002, **74**, 2994–3004.
71 S. L. Das, B. P. Sutherland, E. Lejeune, J. Eyckmans and C. S. Chen, *Am. J. Physiol.*, 2022, **323**, H738–H748.
72 A. Shakeri, S. Khan and T. F. Didar, *Lab Chip*, 2021, **21**, 3053–3075.
73 Y. Qi, Y. Wang, C. Chen, C. Zhao, Y. Ma and W. Yang, *ACS Appl. Bio Mater.*, 2020, **2020**, 3203–3209.
74 Q. Pu, O. Oyesanya, B. Thompson, S. Liu and J. C. Alvarez, *Langmuir*, 2007, **23**, 1577–1583.
75 S. Kuddannaya, Y. J. Chuah, M. H. A. Lee, N. V. Menon, Y. Kang and Y. Zhang, *ACS Appl. Mater. Interfaces*, 2013, **5**, 9777–9784.
76 P. J. Wipff, H. Majd, C. Acharya, L. Buscemi, J. J. Meister and B. Hinz, *Biomaterials*, 2009, **30**, 1781–1789.
77 R. B. Vernon and E. Helene Sage, *J. Cell. Biochem.*, 1996, **60**, 185–197.
78 V. L. Cross, Y. Zheng, N. Won Choi, S. S. Verbridge, B. A. Sutermaster, L. J. Bonassar, C. Fischbach and A. D. Stroock, *Biomaterials*, 2010, **31**, 8596–8607.
79 S. Raz, D. Sheban, N. Gonen, M. Stark, B. Berman and Y. G. Assaraf, *Cell Death Dis.*, 2014, **5**, 1–9.
80 T. Stanković, T. Ranđelović, M. Dragoj, S. Stojković Burić, L. Fernández, I. Ochoa, V. M. Pérez-García and M. Pešić, *Drug Resistance Updates*, 2021, **55**, 100753.
81 S. J. Edwards, V. Carannante, K. Kuhnigk, H. Ring, T. Tararuk, F. Hallböök, H. Blom, B. Önfelt and H. Brismar, *Front. Mol. Biosci.*, 2020, **7**, 1–10.
82 S. Nath and G. R. Devi, *Pharmacol. Ther.*, 2016, **163**, 94–108.